Title

Quantification of elongation stalls and impact on gene expression in yeast.

Journal

RNA, 29(12)

Authors

Hou, Wanfu

Harjono, Vince

Harvey, Alex

et al.

Publication Date

2023-12-01

DOI

10.1261/rna.079663.123

Peer reviewed

Quantification of elongation stalls and impact on gene expression in yeast

WANFU HOU,[1,3] VINCE HARJONO,[1,3] ALEX T. HARVEY,[1] ARVIND RASI SUBRAMANIAM,[2] and BRIAN M. ZID[1]

[1]Department of Chemistry and Biochemistry, University of California San Diego, La Jolla, California 92093, USA

[2]Basic Sciences Division and Computational Biology Section of the Public Health Sciences Division, Fred Hutchinson Cancer Center, Seattle, Washington 98109, USA

ABSTRACT

Ribosomal pauses are a critical part of cotranslational events including protein folding and localization. However, extended ribosome pauses can lead to ribosome collisions, resulting in the activation of ribosome rescue pathways and turnover of protein and mRNA. While this relationship has been known, there has been little exploration of how ribosomal stalls impact translation duration at a quantitative level. We have taken a method used to measure elongation time and adapted it for use in *Saccharomyces cerevisiae* to quantify the impact of elongation stalls. We find, in transcripts containing Arg CGA codon repeat-induced stalls, a Hel2-mediated dose-dependent decrease in protein expression and mRNA level and an elongation delay on the order of minutes. In transcripts that contain synonymous substitutions to nonoptimal Leu codons, there is a decrease in protein and mRNA levels, as well as similar elongation delay, but this occurs through a non-Hel2-mediated mechanism. Finally, we find that Dhh1 selectively increases protein expression, mRNA level, and elongation rate. This indicates that distinct poorly translated mRNAs will activate different rescue pathways despite similar elongation stall durations. Taken together, these results provide new quantitative mechanistic insight into the surveillance of translation and the roles of Hel2 and Dhh1 in mediating ribosome pausing events.

Keywords: translation elongation; ribosome stalling; codon optimality; ribosome quality control; no-go decay

INTRODUCTION

Production of cellular proteins through translation is crucial for maintaining homeostasis and adapting to changing environmental conditions. Translation can be broken down into three sequential steps: initiation, during which ribosomes assemble at the initiation site on an mRNA, elongation, during which ribosomes translocate across the mRNA and build upon a nascent peptide, and termination, during which ribosomes are removed from the mRNA, recycled, and the newly synthesized protein is released. Cells dedicate many resources to the monitoring, regulation, and quality control of protein synthesis as dysregulation may lead to aberrant cellular function and neurological diseases such as ALS (Wang et al. 2016; Bosco 2018).

Each step in the translation process is governed by various regulatory steps. Initiation has long been known to be the rate-limiting step in translation for most mRNAs and subject to intense regulation (Sonenberg and Hinnebusch 2009; Shah et al. 2013). Recent studies have focused on elongation as another important regulatory step in protein synthesis (Stein and Frydman 2019). Indeed, modulation of elongation speed has been shown to serve a functional role in both proper protein folding (Hartl et al. 2011; Spencer et al. 2012; Pechmann and Frydman 2013; Yu et al. 2015; Zhao et al. 2021) and localization (Ogg and Walter 1995; Maton et al. 2000; del Alamo et al. 2011; Tsuboi et al. 2020). These examples give credence to the notion that ribosome pausing is essential for certain cellular processes. Recent reports using ribosome profiling to analyze disome peaks have estimated that upwards of 10% of translating ribosomes are engaged in the disome state (Arpat et al. 2020; Han et al. 2020; Zhao et al. 2021), indicating the commonplace occurrence of ribosome collisions.

The functional and necessary nature of ribosome stalls, however, makes it challenging for cellular machinery to distinguish between beneficial stalls and situations requiring

[3]Co-first author.

Abbreviations: AA, amino acids; ATc, anhydrotetracycline; CDS, coding sequence; miRFP, monomeric infrared fluorescent protein; NGD, no-go decay; nLuc, nanoluciferase; ORF, open reading frame; RLU, relative light unit; RQC, ribosome quality control; WT, wild-type; YFP, yellow fluorescent protein

Corresponding author: zid@ucsd.edu

Article is online at http://www.rnajournal.org/cgi/doi/10.1261/rna.079663.123. Freely available online through the *RNA* Open Access option.

ribosome rescue. Ribosomes that undergo translation on an aberrant mRNA, such as on a truncated mRNA, stall in place and are unable to be disassembled by translation termination machinery (Buskirk and Green 2017; Joazeiro 2017; Yip and Shao 2021). Upon extended stalling events, translating ribosomes may collide with stalled ribosomes, resulting in a ribosome collision which can eventually lead to further accumulation of collided ribosomes. Two pathways may be activated upon the detection of these collision events: (i) ribosome quality control (RQC), which leads to the rescue and recycling of stalled ribosomes, and (ii) no-go decay (NGD), which leads to the endonucleolytic cleavage and subsequent degradation of the aberrant transcript (Ferrin and Subramaniam 2017; Simms et al. 2017; Park and Subramaniam 2019). Both pathways are triggered by the ribosome collision sensor Hel2(yeast)/ZNF598(mammals) which detects disome formations that form as a result of prolonged ribosome stalling (Ikeuchi et al. 2019). In RQC, Hel2 ubiquitinates the small ribosomal subunit which leads to activation of the RQC trigger (RQT) complex in yeast, ultimately resulting in ribosome disassembly and degradation of the nascent peptide (Buskirk and Green 2017; Joazeiro 2017; Yip and Shao 2021). Concurrently, Hel2 activation also leads to the activation of the NGD pathway which results in mRNA degradation primarily through the endonuclease Cue2 and the exonucleases Xrn1 and Ski7 (Buskirk and Green 2017; D'Orazio et al. 2019; Navickas et al. 2020). Hel2 and other sensors of elongation quality must maintain a balance between permitting transient and functional stalls while at the same time engaging rescue pathways to prevent the buildup of ribosomes on problematic mRNA.

How elongation quality sensors can distinguish between functional stalls and those requiring rescue pathways remains unclear. It has been proposed that the severity of ribosome collision may determine which cellular response is activated in response to a collision event (Meydan and Guydosh 2021). Supporting this model, a recent study by Goldman et al. (2021) found that clearance of stalled ribosomes was far slower than elongation and termination and proposed that slow ribosome clearance allows cells to distinguish between transient and deleterious stalls. While this model may explain how functional stalls and detrimental stalls either resume elongation or initiate RQC using the same surveillance pathways, respectively, the definition of "severity" in this context remains vague. Are the distinguishing factors the time duration of the stall, the number of ribosome collisions (Goldman et al. 2021), the specific location and context of where the stall occurs on a transcript, or a combination of all these factors and more? It is from this lack of understanding of how cellular surveillance machinery can distinguish between these two opposing outcomes that necessitates reliable, quantitative methods to describe the various aspects of ribosome stalling events.

One important factor that contributes to elongation speed is codon optimality, a metric that describes the translational efficiency of the 61 amino acid specifying codons. Codon optimality, unique to each species, takes into account various factors implicated in elongation rate, including tRNA availability and demand, frequency of use in the genome, GC content, wobble decoding, and interactions with the ribosome exit tunnel (dos Reis et al. 2004; Pechmann et al. 2013; Gardin et al. 2014; Presnyak et al. 2015). Furthermore, codon optimality has been found to correlate with elongation speed and mRNA decay, with transcripts enriched in "optimal" codons associated with faster elongation speed and lower mRNA decay rates and those enriched in "nonoptimal" codons associated with slower elongation speed and higher mRNA decay rates (Ingolia et al. 2009; Chu et al. 2011; Gardin et al. 2014; Ingolia 2014; Hussmann et al. 2015; Koutmou et al. 2015; Harigaya and Parker 2016; Radhakrishnan et al. 2016; Saikia et al. 2016; Weinberg et al. 2016; Hanson and Coller 2018). While many studies, both in vivo and in vitro, have assessed the impact of synonymous codon substitutions on protein expression, mRNA decay, and ribosome pausing, quantification of the impact on elongation time has not been widely available.

In this study, we describe the development of an in vivo quantitative luciferase-based assay to measure elongation time. We assessed the time delay associated with acute stalls caused by the inclusion of repeats of the nonoptimal arginine codon CGA and find that elongation time increases in a dose-dependent manner. Surprisingly, we find that no-go RNA decay reaches a maximum level at a specific stall length despite increasing translation elongation times and protein expression continuing to decrease. Furthermore, we assessed the effect of synonymous codon substitutions on elongation time of a standardized ORF and identified the nonoptimal leucine codon CTT as a strong driver of elongation delay. CTT's effect on elongation time was context dependent as only specifically localized nonoptimal CTT's caused significant elongation delays and protein repression. The development of this assay and our findings provide steps toward a detailed understanding of the triggers of RQC pathways.

RESULTS

Development and validation of elongation assay

To create a quantitative elongation duration reporter assay, we utilized a tetracycline-inducible promoter to control mRNA induction of a bioluminescent nanoluciferase (nLuc) reporter downstream from open reading frames (ORFs) of interest. The nLuc reporter has been previously studied in yeast under the control of a stress-inducible promoter, and its bioluminescent output faithfully recapitulates induced mRNA levels after heat shock (Masser et al.

2016). To test this system, we developed a series of constructs in which we varied the length of the upstream ORF by insertion of yeast-optimized yellow fluorescent protein (YFP) or yeast-optimized monomeric infrared red fluorescent protein (miRFP) ORFs upstream of nLuc (Fig. 1A). Tet-nLuc is included to control for the time cost of initiation steps including anhydrotetracycline (ATc) penetration, transcription initiation, mRNA export, and translation initiation. nLuc protein expression was collected for each construct over 60 min and normalized to OD600 measured at $T = 0$ min (time of ATC addition). Elongation time was calculated using a Schleif plot (Schleif et al. 1973) and adjusted based on an average mRNA transcription time of 1500 nt per minute (Edwards et al. 1991; Mason and Struhl 2005). We find a delay in the first appearance of nLuc upon the addition of optimized YFP (optYFP) and a further delay in the longer miRFP-optYFP-nLuc reporter (Fig. 1B). We then used these measured delays to calculate the translation elongation rate of optYFP and miRFP ORFs as ~4 AA/sec and 3 AA/sec (Fig. 1C), respectively, which is consistent with bulk elongation rate measurements of 3–10 AA/sec (Karpinets et al. 2006; Riba et al. 2019). We do not find a significant difference in elongation rate between the two optimized ORFs. This implies that our reporter can quantify the in vivo translation rates of our reporters.

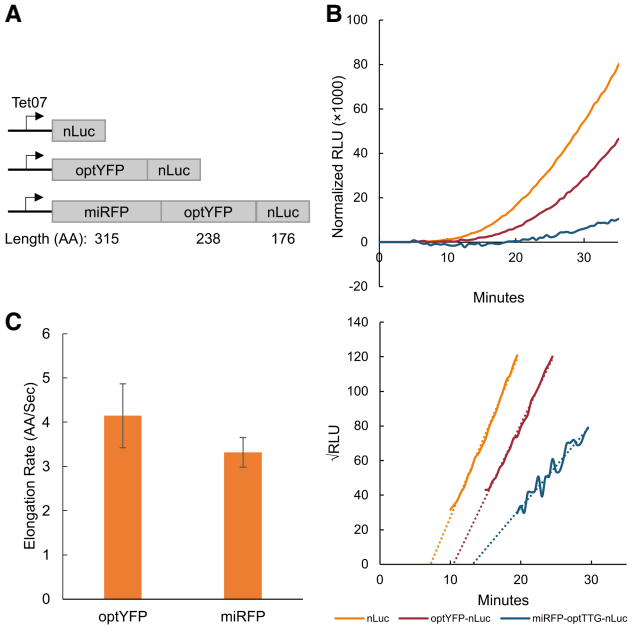

FIGURE 1. Assay validation via elongation rate measurements. (*A*) Diagram of yeast-optimized constructs of various lengths. optYFP or both optYFP and optimized miRFP (miRFP) are set upstream of an nLuc reporter. Constructs are expressed from an inducible Tet07 promoter. (*B, top*) Representative assay data of relative light units (RLU) of each construct over time normalized to OD600. (*Bottom*) Schleif plot and associated trendlines of the *top* graph. (*C*) Calculated elongation rate measurements of optYFP ($n = 9$) and miRFP ($n = 4$) ORFs. Error bars indicate SEM.

Hel2 decreases protein expression, mRNA levels, and delays elongation in acute CGA constructs

To further explore the utility of our reporter, we wanted to verify that this system could quantify the duration of elongation pauses of known ribosome stalling sequences. Consecutive nonoptimal CGA arginine codons are known to induce slow translation elongation and terminal stalling through wobble decoding of CGA (Letzring et al. 2010; Tsuboi et al. 2012; Tesina et al. 2020; Veltri et al. 2022). To quantify the effect of these nonoptimal codons on elongation time and gene expression, we developed a series of constructs in which we inserted between two and six tandem CGA repeats between the yeast-optYFP ORF and nLuc reporter ORF shown previously (Fig. 2A). First, we tested the protein expression of our induced constructs and found a dose-dependent exponential decline in protein production as the number of CGA codons increased, similar to a previous study by Letzring et al. (2010) (Fig. 2B). However, we did not see a significant impact on protein expression until three CGA codons were included. Next, we measured mRNA levels and found that mRNA levels significantly decreased with the addition of three CGA codons, but mRNA levels remained constant around 40% of our control construct regardless of additional CGA codons (Fig. 2C). We then measured the elongation delay in each of our constructs by comparing to a control reporter lacking any CGA codons (Fig. 2D). We found that elongation delay increased in a dose-dependent manner beginning at 3×CGAs, with 6×CGA causing an ~4.5 min extension of the translation duration. There was a relatively linear relationship between CGA stall number after three CGAs and elongation time, which allowed us to calculate that each CGA adds ~76 sec to the overall elongation time. We found that this elongation delay was specifically due to CGA codons as a 6×AGA codon, which also encodes for arginine, had no effect on elongation time (Supplemental Fig. 1).

We then tested the role of Hel2 and Syh1, two factors implicated in impacting gene expression due to prolonged ribosome stalls. Hel2 is a translation surveillance factor that senses ribosome collisions and activates the ribosome rescue pathways RQC and NGD, which results in protein and mRNA turnover, respectively. Syh1 is a homolog of the mammalian NGD factor GIGYF1/2 that was previously found to have a role in NGD in yeast (Hickey et al. 2020; Veltri et al. 2022). We measured protein expression in our constructs containing two, four, and six CGAs in a *hel2Δ* background and six CGAs in a *syh1Δ* background, and we compared it to their wild-type (WT) counterparts (Fig. 3A; Supplemental Fig. 2). We found that deletion of Hel2 partially rescued protein expression in the 4×CGA and 6×CGA, but *SYH1* deletion had no effect on the 6×CGA protein expression. We next measured RNA levels in our 2×CGA, 4×CGA, and 6×CGA strains and found that RNA levels were increased in our 4×CGA and 6×CGA-

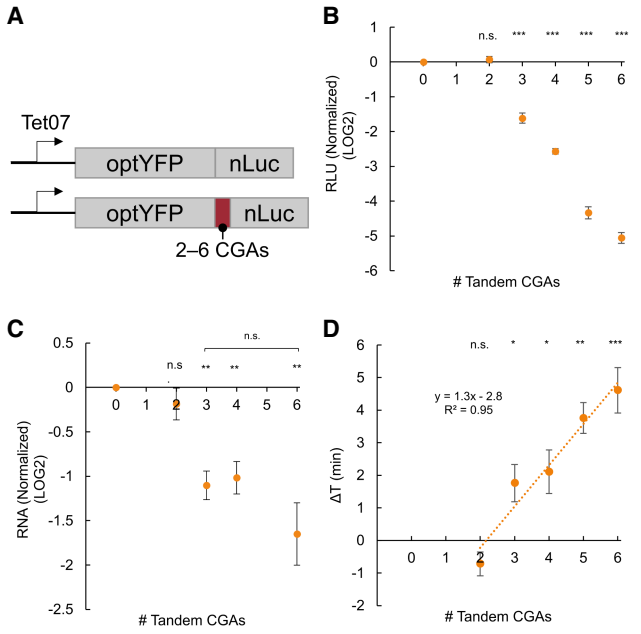

FIGURE 2. CGA-derived acute stalls negatively impact gene expression and increase elongation time in a dose-dependent manner. (*A*) Diagram of optimal and CGA-containing constructs. Between two and six CGAs are inserted between the optYFP and nLuc ORFs. (*B*) Protein expression of CGA constructs at $T = 60$ min normalized to optimized control (2×CGA $n = 10$, 3×CGA $n = 8$, 4×CGA $n = 10$, 5×CGA $n = 5$, 6×CGA $n = 10$). (*C*) mRNA levels of CGA constructs at $T = 60$ min normalized to optimized control ($n = 3$). (*C*) Elongation delay of CGA-containing constructs compared to optimized control ($n = 3$). All error bars indicate SEM. All statistical significances were calculated for each construct using two-tailed paired Student's *t*-test against optYFP control.

containing *hel2Δ* strains, but there was no change in the 2×CGA strain (Fig. 3B). We found no significant difference in RNA levels for the 6×CGA in our *syh1Δ* strain (Supplemental Fig. 2B). Together, these results imply Hel2-mediated RQC and NGD are partially responsible for the observed decrease in protein and RNA levels, respectively, in the WT strains. Lastly, we sought to measure the impact of Hel2 on elongation time. A recent review by Meydan and Guydosh (2021) proposed two nonmutually exclusive models of Hel2's activity on the stability of ribosome collisions: (i) Hel2 is necessary to rescue stalled ribosomes and Hel2 deletion would result in further buildup of collided ribosomes, and (ii) Hel2 stabilizes collided ribosomes and Hel2 deletion would result in reduced ribosomal pausing. Model 2, in which Hel2 stabilizes collided ribosomes, was further supported by experimental data that *hel2Δ* reduces disome pauses in ribosome profiling data sets (Meydan and Guydosh 2020). To assess the effect of Hel2 on elongation time and distinguish between these two models, we compared the elongation time of our control, 4×CGA, and 6×CGA strains between WT and *hel2Δ* backgrounds and found no significant difference in our control strain, but a decrease in overall elongation time in our 4×CGA and 6×CGA strains when expressed in a *hel2Δ* background (Fig. 3C). This suggests that Hel2 functions to slow down elongation in our CGA-containing strains and is consistent with the second proposed model in which Hel2 stabilizes collided ribosomes.

Synonymous substitution to nonoptimal codons negatively impacts gene expression

Next, we asked how distributed slowdowns of nonoptimal codons impact gene expression and elongation time. To study the impact of distributed nonoptimal codons, we used our optYFP-nLuc construct and synonymously substituted the first 20 of 21 leucines for a nonoptimal leucine variant (Fig. 4A; Supplemental Fig. 3). First, we wanted to determine the impact of these synonymous substitutions on overall elongation time. We measured the elongation time in each of our strains and compared it to the optimized strain to determine the elongation time delay associated with each synonymous substitution (Fig. 4A). We found that substitution of the optimal leucine codon TTG with the nonoptimal codons CTC and CTT resulted in a significant delay in elongation time of ∼0.5 and 2.5 min, respectively (Fig. 4B). Due to the statistically significant differences in elongation time, we selected both the CTC and CTT-containing constructs for further study. Next, we measured the impact of codon substitution on protein and RNA levels (Fig. 4C,D). As compared to the optimized control, we determined that substitution to the CTC codon reduced both protein and mRNA levels by ∼20%, and substitution to the CTT codon reduced both protein and mRNA levels by 50%. This was distinct from the RQC-inducing CGA stalls that decreased protein production more substantially than they did mRNA levels.

We sought to determine whether the increase in elongation time and decrease in protein expression observed was either contributed equally by each nonoptimal codon or the specific placement of nonoptimal codons in the YFP ORF. To assess this, we created a set of chimeric reporters in which the first 10 leucine codons in the YFP ORF were either optimal or nonoptimal followed by the next 10 leucine codons of the opposite optimality (Fig. 4A). We hypothesized that if each codon contributed equally to elongation time, the elongation time delay of our chimeric constructs would be half of the delay between optYFP and YFP[CTT]. Instead, we found that both the elongation delay and protein expression of our chimeric YFP[1–10CTT] closely resembled YFP[CTT], and that our chimeric YFP[11–20CTT] closely resembled YFP[TTG] (Fig. 4E,F). This provides evidence that substitution of leucine codons to a nonoptimal variant in the 5′ half of the YFP ORF is sufficient to drive protein expression and elongation time outcomes.

A previous study by Chu et al. (2014) showed that poor codons in the 5′ region of a transcript could negatively affect translation initiation through ribosome buildup preventing

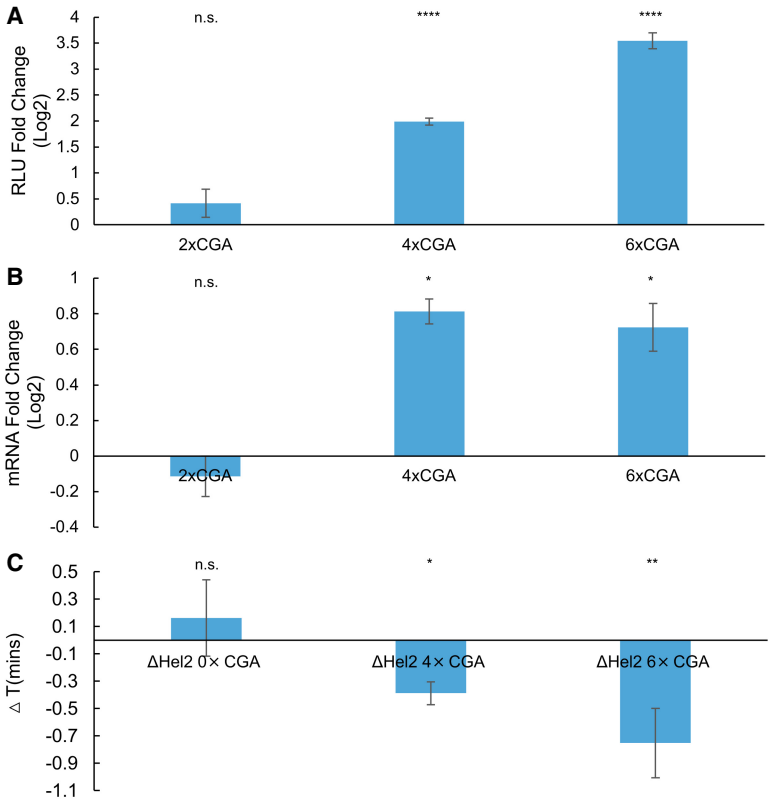

FIGURE 3. Hel2 deletion rescues protein expression, mRNA levels, and elongation time. (*A*) Protein expression fold change of CGA constructs in a *hel2Δ* versus WT background (2×CGA $n = 2$, 4×CGA $n = 7$, 6×CGA $n = 7$). (*B*) mRNA level fold change of CGA constructs in a *hel2Δ* versus WT background ($n = 3$). (*C*) Elongation delay of CGA constructs in a *hel2Δ* versus WT background ($n = 3$). All error bars indicate SEM. All statistical significances were calculated for each construct using two-tailed paired Student's *t*-test against WT control.

initiation from occurring, thereby reducing overall translational output (Hanson and Coller 2018). To test if the observed decrease in protein expression was a result of interference with initiation, we inserted a yeast-optimized miRFP (315 amino acids) upstream of our optYFP-nLuc and YFP[CTT]-nLuc constructs. We hypothesized that if initiation was negatively impacted by ribosome buildup, addition of a long yeast-optimized ORF upstream of the nonoptimal YFP [CTT] would rescue protein expression as compared to the optimal construct. Instead, we found that a statistically significant difference remained between the optimal and CTT-containing nonoptimal constructs (Supplemental Fig. 4A). Furthermore, we assessed the impact on elongation time and found that elongation time was not rescued to WT levels and the magnitude of delay is similar to the YFP[CTT] construct (Supplemental Fig. 4B). This suggests that the decrease in protein expression in the reporter is a result of the specific placement of the nonoptimal CTT codons within the 5′ half of the YFP ORF, but does not depend on the nonoptimal codons to be near the initiation codon.

To further dissect which leucine codons were important for the repression of protein expression, we made constructs that contained diminishing numbers of CTT codons from the first 10 leucine codons. We found that the first eight and nine codons showed similar levels of protein reduction, but the first seven leucine codons as CTT did not diminish expression (Fig. 4F). Because the switch took place from the seventh to eighth leucine codons, we tested whether the eighth leucine codon as a nonoptimal CTT codon was sufficient to see the full effects. We found that a single CTT at the eighth leucine codon did not significantly alter elongation time or protein expression relative to the optimal YFP control (Fig. 4E,F). We did, however, find that only two leucine codons, 7 and 8, at amino acid positions 60 and 64, respectively (Fig. 4A), switched to CTT were sufficient to fully repress protein expression and elongation time (Fig. 4E,F). The switching of leucines 7 and 8 from TTG to CTT was associated with a more strongly folded local stem–loop structure as predicted by mFold (Supplemental Fig. 5B). To test if local RNA structure was important to the increased elongation time and reduction in protein production, we made synonymous mutations to G65 from GGT to GGC and T62 from ACT to ACA. According to mFold these mutations reduce local base pairing, making a weaker and finally disfavored predicted stem–loop (Supplemental Fig. 5C). Even though the Leu CTT 7 and 8 codons are kept constant, we find the GGT-GGC + ACT-ACA mutations cause a significant reduction in the elongation time and rescue of protein expression relative to YFP[7,8 CTT] (Fig. 4E,F). These data point to the importance of a local stem–loop structure in affecting translation duration.

Gene expression in nonoptimal codon constructs is affected by deletion of *DHH1* but not *HEL2*

Finally, we investigated if Hel2 or other translation sensors were responsible for the negative impacts on gene expression in our YFP[CTT] constructs. Of particular interest was the RNA binding protein Dhh1, a conserved DEAD-box helicase previously shown to have roles in mRNA decapping and translational repression (Coller et al. 2001; Fischer and Weis 2002; Tseng-Rogenski et al. 2003; Carroll et al. 2011). Importantly, it has been shown to bind preferentially to mRNA with low codon optimality and has been

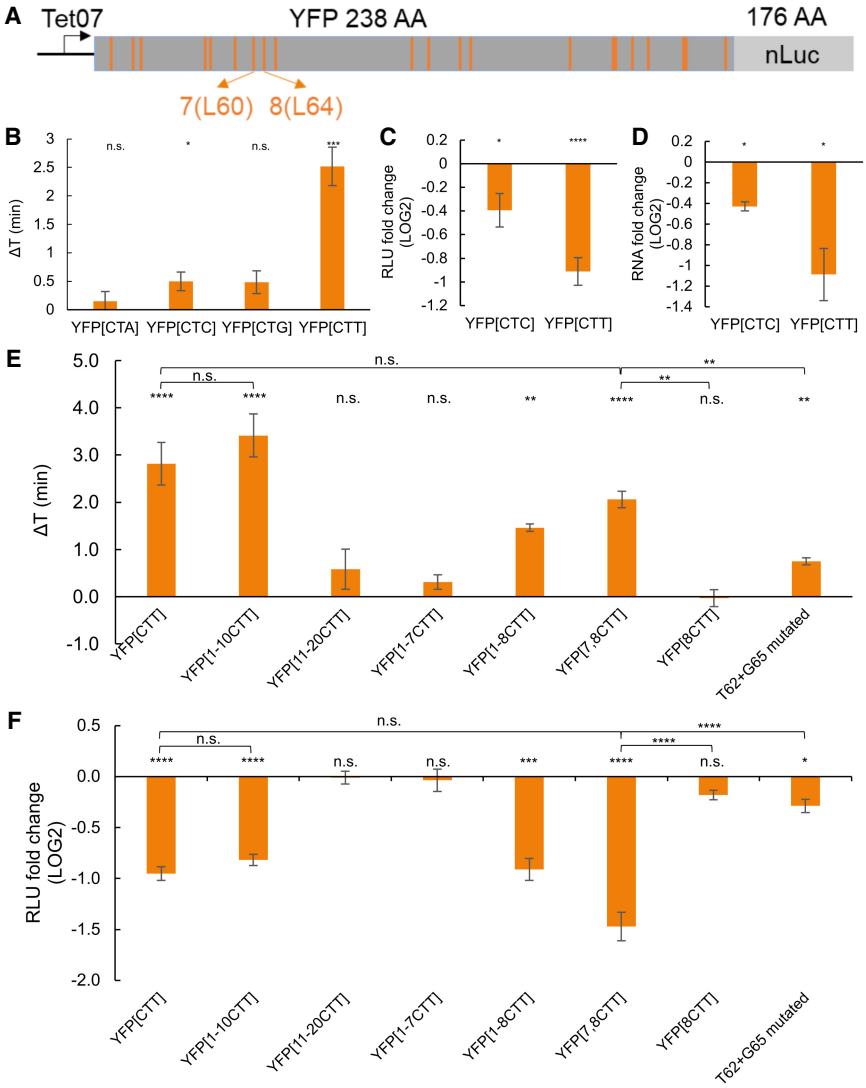

FIGURE 4. Distributed stalls in the YFP ORF decrease protein expression, mRNA levels, and delays elongation time. (*A*) Diagram of synonymously substituted leucine constructs. YFP contains 21 leucine codons which are marked in orange. The first 20 leucine codons are substituted for a nonoptimal leucine variant, and the 21st leucine remains the optimal TTG codon. No. 7 and no. 8 leucines from the 5′end of YFP ORF are labeled as L60 and L64. (*B*) Elongation delay of distributed stall constructs compared to optYFP (YFP[CTA] $n = 6$, YFP[CTC] $n = 6$, YFP[CTG] $n = 5$, YFP[CTT] $n = 7$). The first 20 out of 21 total optimal TTG leucine codons in optYFP are synonymously substituted to a nonoptimal codon specified in brackets. (*C*) Protein expression of distributed stall constructs normalized to optYFP control ($n = 4$ for all). (*D*) mRNA levels of distributed stall constructs normalized to optYFP control ($n = 3$ for all). (*E*) Elongation delay measurements of chimeric constructs normalized to optYFP control ($n = 3$ for YFP[1–7CTT], YFP[1–8CTT], YFP[8CTT], and T62 + G65 mutated constructs, $n = 5$ for YFP[1–10CTT] and YFP[11–20CTT], $n = 11$ for YFP[CTT], $n = 12$ for YFP[7,8CTT]). (*F*) Protein expression chimeric constructs normalized to optYFP control ($n = 3$ for YFP[1–7CTT], YFP[1–8CTT], YFP[8CTT], and T62 + G65 mutated constructs, $n = 5$ for YFP[1–10CTT] and YFP[11–20CTT], $n = 11$ for YFP[CTT], $n = 12$ for YFP[7,8CTT]). All error bars indicate SEM. All statistical significances were calculated for each construct using two-tailed paired Student's *t*-test against optYFP control unless otherwise specified.

proposed to slow down ribosome movement (Sweet et al. 2012; Radhakrishnan et al. 2016). We hypothesized that the negative impacts on gene expression observed in YFP[CTC] and YFP[CTT] compared to the optYFP control may be a result of either Hel2 or Dhh1 influence. To test this, we transformed our optYFP, YFP[CTC], and YFP[CTT] constructs into either a *dhh1Δ* or *hel2Δ* strain.

First, we assessed the impact of protein expression on our constructs in a *dhh1Δ* or *hel2Δ* strain deletion background (Fig. 5A). Based on Dhh1's role in mediating translation repression of transcripts enriched in nonoptimal codons, we expected to see no impact in optYFP and a rescue of protein expression in YFP[CTC] and YFP[CTT]. Instead, we found differing effects for each construct; deletion of Dhh1 slightly increased protein expression in our optYFP construct, decreased protein expression in our YFP[CTC] construct and had no statistically significant impact in our YFP[CTT] construct. We also found that Hel2 deletion had no statistically significant effect on protein expression in any of our constructs (Fig. 5A). This suggests that the drop in protein expression seen in the YFP[CTT] constructs was not due to a Hel2-mediated mechanism and is distinct from our acute CGA-containing constructs. Next, we examined the effect of Dhh1 on mRNA levels by comparing WT and *dhh1Δ* mRNA levels (Fig. 5B). We found that deletion of Dhh1 decreased mRNA levels in our YFP[CTC] construct but had no statistically significant difference in the other constructs. The negative impact of Dhh1 deletion in our YFP[CTC] construct was of similar magnitude in protein and mRNA. This suggests that Dhh1 increases mRNA levels in our YFP[CTC] construct, which leads to increased protein expression.

Lastly, we wanted to determine the impact of *dhh1Δ* and *hel2Δ* backgrounds on elongation time in our substituted leucine constructs. We measured elongation delay by comparing the elongation times of our constructs in each deletion strain to WT (Fig. 5C). We found that deletion of Dhh1 slightly increased the elongation delay in our optYFP and more dramatically increased the elongation delay in the YFP[CTC]

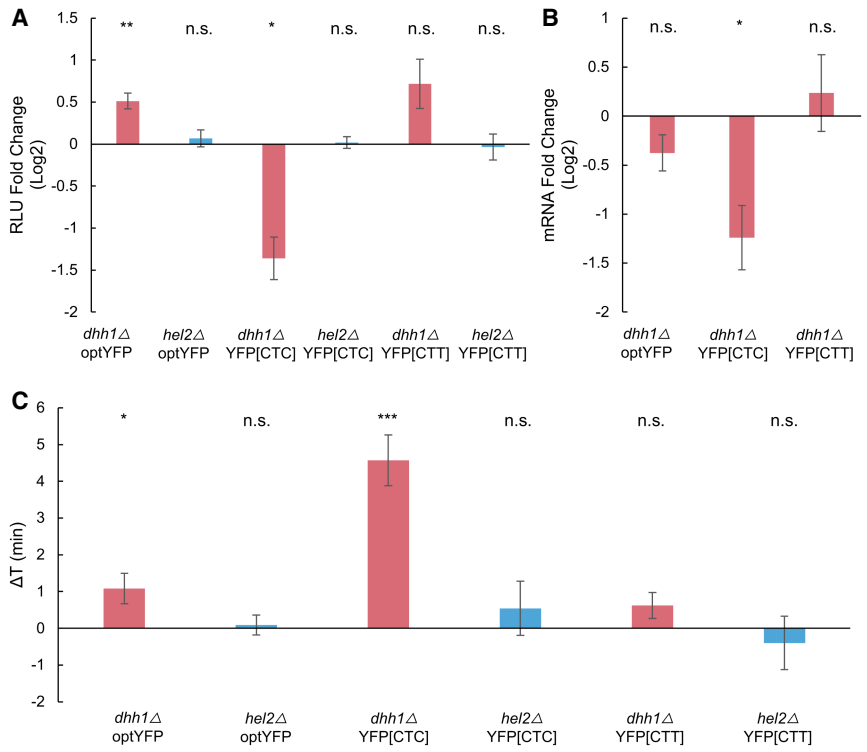

FIGURE 5. Dhh1 deletion, but not Hel2 deletion, affects gene expression in substitution constructs. (*A*) Protein expression of distributed stall constructs in *dhh1Δ* or *hel2Δ* background versus WT ($n = 5, 4, 5, 6, 7$, and 3 from *left* to *right*). (*B*) mRNA level fold change of distributed stall constructs in a *dhh1Δ* versus WT background ($n = 5$, 5, and 7 from *left* to *right*). (*C*) Elongation delay of distributed stall constructs in *dhh1Δ* or *hel2Δ* background versus WT ($n = 19, 4, 18, 6, 9$, and 5 from *left* to *right*). All error bars indicate SEM. All statistical significances were calculated for each construct using two-tailed paired Student's *t*-test against WT control.

strain, suggesting that Dhh1 functions to speed up elongation in these constructs. However, we found no statistically significant difference in elongation time in our YFP[CTT] construct. Additionally, we found no statistically significant difference in elongation times in our *hel2Δ* strains (Fig. 5C). This is consistent with the *hel2Δ* strain protein expression data and supports the idea that a non-Hel2-mediated pathway is responsible for the negative impact on gene expression in our substituted leucine constructs.

DISCUSSION

Ribosome stalling and the connected quality control pathways are important for recognizing faulty and damaged mRNAs, yet quantitative measurements of how these stalls impact translation duration have been lacking. In this study, we developed a reporter assay to quantify the in vivo elongation time of various constructs containing stalling sequences in *Saccharomyces cerevisiae*. Using CGA stalling reporters we find that total elongation time increases in a dose-dependent manner corresponding with the number of tandem CGA repeats while protein expression decreases logarithmically with increasing CGA repeats. Strikingly, we find that mRNA levels stabilize upon reaching a specific stall length, suggesting that the stall-activated NGD pathway reaches a maximum decay rate at 3×CGA. Interestingly the ∼50% reduction in mRNA levels is very similar to the mRNA reduction seen from a completely independently designed reporter containing 12×CGA (Veltri et al. 2022) and other reporters containing 10×AAG (rare poly-lysine) or 8×CCG (rare poly-proline codon) stalling sequences (Park and Subramaniam 2019), further supporting that NGD may be saturated at relatively shorter translational stalls.

While initially 20 synonymous Leu codons were changed to poor CTT codons, not all nonoptimal codons contribute equally to the elongation slowdown. Instead, we determined that two of the 20 codons were sufficient to drive the full elongation slowdown and repressed protein expression. This appears to be caused by local sequence effects and not specifically the poor codons being in the 5′ end of the ORF, as adding an upstream miRFP ORF was not able to rescue the translation slowdown and reduced protein production. This argues that local sequence context is important for determining the effects of codon optimality on gene expression. This fits with reports showing that specific combinations of codons modulate translation efficiency and mRNA decay (Gamble et al. 2016; Burke et al. 2022). We find that these two CTT substitutions drive the formation of a predicted stem–loop structure and that disruption of this structure, while maintaining the two nonoptimal CTT codons predominantly rescues the slowed translation elongation and reporter expression. Interestingly it was recently shown in prokaryotes that mRNA stem–loops can dock into the A site of the ribosome inhibiting translation elongation and stalling ribosomes in a primarily nonrotated confirmation (Bao et al. 2020, 2022). These works showed that ribosome slowing was due to specific length and structure rather than the high thermodynamic stability of the stem–loop. It will be interesting to further explore if a similar mechanism of translation elongation slowing takes place in eukaryotes.

From our synonymous leucine substitution constructs, we find that the nonoptimal codon CTT causes substantial delays in elongation time on the order of minutes, lengthening the elongation time of YFP ∼3.5-fold. The elongation

delay of ∼150 sec for the CTT reporters, including the 7,8 CTT, is similar to the elongation delay for our 4×CGA stalling reporter. Yet these two reporters behave very differently as the decrease in protein expression due to CTT could be explained completely by decreased mRNA levels, while the 4×CGA decreased protein levels to an even larger extent then the ∼50% decrease in mRNA levels. This pointed to the induction of RQC, which reduces protein expression on the CGA stalls through ribosome rescue. Further supporting this induction of RQC on CGA stalls but not CTT stalls, deletion of the RQC factor Hel2 could partially rescue the mRNA levels and protein production of CGA stalls, yet it had no significant effect on protein production and elongation times due to nonoptimal CTT codons, which we believe is due to the formation of a stem–loop structure. These data point to further differentiation of ribosome stalling beyond just stall duration timing. This fits with previous reports that not all stalled ribosomes are targets for RQC, but instead, the ribosomes need to be in a rotated state to be recognized by Hel2 (Matsuo et al. 2017; Ikeuchi et al. 2019).

We found that CGA stalls added ∼76 sec per CGA codon to the translation duration of the reporter after 3×CGAs. This led to an almost 5 min lengthening of translation duration for a 6×CGA construct. A recent paper by Goldman et al. (2021) examined ribosomal clearance times on mRNA containing difficult-to-translate poly(A)-containing stretches and found it took ∼10 and 13 min for ribosomes to clear off 50% of transcripts containing poly(A)36 and poly(A)60 stretches, respectively. Their finding on delays lasting on the order of minutes is consistent with our findings and represents an intriguing observation considering that the average half-life of yeast mRNAs is ∼10 min, suggesting that a significant portion of an mRNA's half-life can be spent engaged in a ribosomal stall (Chan et al. 2018). The long duration of stalling also fits with long queues of ribosomes 5′ of the stall, as has been seen with disome-seq and in vivo translational imaging in mammalian cells (Han et al. 2020; Goldman et al. 2021). We believe we may be observing a cumulative effect of ribosome queuing affecting the overall translation duration.

It is well-confirmed that Hel2 is a necessary factor mediating RQC and NGD pathways; however, its effects on ribosome stalling have been unclear. Two nonmutually exclusive models have been proposed (Meydan and Guydosh 2020, 2021): first, since Hel2 is needed to promote the rescue of the stalled ribosome in a collision complex, deletion of Hel2 will slow ribosome rescue, resulting in accumulated collided ribosomes, which increases elongation delay; in the second model, as proposed by Meydan and Guydosh, Hel2 is able to sense and stabilize stalled ribosomes to prevent further translation. In this scenario, deletion of Hel2 would destabilize collided ribosomes, resulting in rescued elongation and shorter elongation delay. In this paper, we quantitatively measure the change of elongation delay after Hel2 depletion and find a reduction in the translation duration of CGA stalled sequences. This is distinct from mammalian cells, where depletion of the mammalian homolog of Hel2, ZNF598, causes further delays in the clearing of ribosomes (Goldman et al. 2021).

It has been previously reported that Dhh1 plays a role in the degradation of mRNA enriched in nonoptimal codons (Radhakrishnan et al. 2016). We were surprised to find that Dhh1 deletion instead decreases the expression of the YFP [CTC] construct. As the YFP constructs used in this study are all yeast optimized except for the leucine codons, it is possible that Dhh1 deletion would only be beneficial for mRNAs more enriched in poor codons. Previous work demonstrates a negligible effect of *dhh1Δ* on mRNA half-life for primarily optimal mRNA (Radhakrishnan et al. 2016).

Although most studies have investigated Dhh1 with regards to its role in mRNA decay and translational repression, Dhh1 has also been shown to promote the translation of certain mRNAs. It has been previously demonstrated that a subset of mRNAs that contain structured 5′UTRs and coding sequences require Dhh1 helicase activity for efficient expression (Jungfleisch et al. 2017). Furthermore, Dhh1 can shift roles in a condition-dependent manner. During nitrogen starvation, Dhh1 is required for the efficient expression of autophagy-related proteins Atg1 and Atg13, but when nutrients are plentiful Dhh1 encourages ATG mRNA degradation (Liu et al. 2019). Overall, this argues that Dhh1 may play context-specific roles in translation elongation and may be able to speed up elongation in specific sequence contexts.

MATERIALS AND METHODS

Plasmid preparation and integration

All plasmids used in this study are listed in the Supplemental Data File. A number of the key elongation reporter plasmids have been deposited at Addgene (www.addgene.org/Brian_Zid/). Plasmids containing synonymous leucine codons substituted YFP (TTG, CTA, CTC, CTG, and CTT), and single-copy yeasts integrating plasmid containing a pTET07 promoter were provided as a kind gift from Dr. Arvind Rasi Subramaniam at the Fred Hutchinson Cancer Center in Seattle. Fragments containing pTET07, YFP variants, and yeast-optimized nLuc (Promega cat. no. N1141) were amplified using PCR and cloned into the XhoI and HindIII-digested single-copy yeast integrating plasmid using Gibson assembly.

The pAG306-pTet07-YFP[1–7CTT]-nLuc, pAG306-pTet07-YFP[1–8CTT]-nLuc, pAG306-pTet07-YFP[1–9CTT]-nLuc, pAG306-pTet07-YFP[1–10CTT]-nLuc, and pAG306-pTet07-YFP[11–20CTT]-nLuc strains were generated by PCR amplification of the entire backbone of the previous pAG306-pTet07-YFP[TTG]-nLuc plasmid beginning at nLuc and ending with pTet07, and PCR amplification of the corresponding parts of the YFP[TTG] and YFP[CTT] variants (e.g., YFP[1–7CTT] includes nos. 1–7 Leu codon part of YFP[CTT] and nos. 8–20 Leu codon part of YFP

[TTG]) (Supplemental Fig. 5A). These fragments were combined using Gibson assembly.

The pAG306-pTet07-YFP[7,8CTT]-nLuc and pAG306-pTet07-YFP[8CTT] were further constructed with the same backbone of the pAG306-pTet07-YFP[TTG]-nLuc plasmid and distinct YFP variants. YFP[7,8CTT] and YFP[8CTT] variants are constructed based on YFP[TTG] and YFP[1–8CTT] (e.g., YFP[7,8CTT] includes nos. 1–6 Leu codon part of YFP[TTG] and nos. 7–20 Leu codon part of YFP[1–8CTT]) (Supplemental Fig. 5A). These fragments were combined using Gibson assembly.

Plasmid variants containing two to six CGA stalls were generated using the aforementioned backbone PCR of the pAG306-pTet07-YFP[TTG] plasmid and a PCR amplified YFP[TTG] fragment containing two to six CGA repeats as a 3′ overhang. These fragments were combined using Gibson assembly.

All plasmids were linearized using NotI and integrated into yeast by homologous recombination. Integrations were screened by growing transformed yeast on synthetic complete (SC) dropout plates lacking uracil. These were then frozen down for long-term storage in YPD containing 15% v/v glycerol.

Yeast strains, growth, and media

The background yeast strain w303 (EY0690) was used for all experiments. Yeast *dhh1Δ*, *hel2Δ*, and *syh1Δ* strains were created by deleting the endogenous DHH1, HEL2, and SYH1 loci, respectively, using pRS315 (Addgene Plasmid #3974) and screened by growing transformed yeast on SC dropout plates lacking leucine. The specific oligos used are listed in Supplemental Table S2.

Luciferase-based elongation reporter assay

Liquid cultures were started from single colonies and allowed to grow overnight in YPD at 30°C with shaking until an approximate OD_{600} of 0.3–0.5, after which cultures were divided into two tubes. For one of the tubes, 1 µL of a stock solution of ATc (250 µg/mL of ATc dissolved in EtOH) was added per mL of culture. Both tubes were returned to 30°C with shaking for 5 min. A total of 90 µL of each culture was added to a 96-well white flat-bottom plate (Grainger), and to each well, 10 µL of furimazine (10 mM furimazine stock solution dissolved in DMSO diluted 1:200 in YPD) was added. Immediately after sample loading, the plate was placed in a 30°C prewarmed Tecan Infinite 200 PRO plate reader. The following program was used and luminescence measurements were taken every 30 or 60 sec: (i) kinetic cycle: (cycle duration: 60 min, kinetic interval: 30 or 60 sec); (ii) shaking: (duration: 3 sec, mode: orbital, amplitude: 2 mm), (iii) luminescence: (attenuation: automatic, integration time: 1000 msec, settle time: 0 msec).

Schleif plot and elongation delay measurements

The Schleif plot methodology was adapted from Schleif et al. (1973) and slightly modified to assume a nonconstant basal expression protein level. The general principle is that upon sufficient time for transcriptional induction to start, there will be a proportional increase in mRNA levels to time (t). The increase of luciferase from a single mRNA is also proportional to time (t). As mRNA levels are also increasing with time, this means that the total amount of luciferase is proportional to t^2. For each sample, ATc-induced protein expression was calculated by subtracting the samples lacking ATc (−ATc) from the corresponding samples with ATc (+ATc) across all measured time points. Samples were then normalized to an OD_{600} of 1.0 by dividing their protein expression over time by their respective ODs. All values were then subtracted by the average RLU of the first 5 min to subtract background. Then, the square root of each value $\sqrt{[(\text{Luc}(t) - \text{Luc}(0)]}$ was calculated and plotted against time. Values that produced an error due to the square root of a negative value were set as "N/A" and avoided in our analysis. From this Schleif plot, we identified regions of linearity across our samples and selected a 10–15 min window for analysis. Ideally, these regions of linearity are parallel between each sample and contain a minimal amount of noise. For each time window, we created a trendline and calculated the X-intercept of the trendline, which represented the calculated elongation time of the sample. The calculated elongation time of the samples in a single assay was then compared to a control to determine the elongation delay. These elongation delay measurements were then compared across assays and aggregated to determine the average elongation delay associated with the specific construct. More details and protocols of the Schleif plot and elongation delay measurements are shown in the Supplemental Schleif Plot Method file.

RNA extraction and real-time qPCR

Yeast pellets were collected from samples 60-min post-ATc addition by spinning 1–1.5 mL of liquid culture at 3000*g* for 2 min and discarding the supernatant. These yeast pellets were then flash frozen in liquid nitrogen and stored at −80°C until RNA extraction. RNA was extracted from yeast pellets using the MasterPure Yeast RNA Purification Kit (Lucigen cat. no. MPY03100), according to the manufacturer's instructions. RNA quality and concentration were assessed using a Nanodrop.

RNA samples were subjected to DNase digestion using RQ1 RNase-free DNase (Promega), according to the manufacturer's instructions. cDNA was prepared from equal amounts of RNA from each sample using Protoscript II Reverse Transcriptase (New England Biolabs cat. no. M0368X) and an oligo dT(18) primer according to the manufacturer's instructions. RT-qPCR was done using a homebrew recipe with SYBR Green at a final concentration of 0.5× (Thermo Fisher S7564). Primers specific for nLuc and actin are described in Supplemental Table S2. mRNA levels were normalized to ACT1 abundance, and fold change was calculated by a standard C_t analysis.

SUPPLEMENTAL MATERIAL

Supplemental material is available for this article.

ACKNOWLEDGMENTS

We would like to thank the Zid laboratory for helpful feedback on this manuscript. We thank Claes Andréasson for sharing the yeast-optimized Nanoluciferase. This work was supported in part by the National Institutes of Health R35GM128798 (B.M.Z.), funding from the UCSD Molecular Genetics Training grant (V.H.), and a training grant in Quantitative Integrative Biology from UCSD's qBio Program (A.T.H.).

Received March 16, 2023; accepted September 21, 2023.

REFERENCES

Arpat AB, Liechti A, de Matos M, Dreos R, Janich P, Gatfield D. 2020. Transcriptome-wide sites of collided ribosomes reveal principles of translational pausing. *Genome Res* **30:** 985–999. doi:10.1101/gr.257741.119

Bao C, Loerch S, Ling C, Korostelev AA, Grigorieff N, Ermolenko DN. 2020. mRNA stem-loops can pause the ribosome by hindering A-site tRNA binding. *Elife* **9:** e55799. doi:10.7554/eLife.55799

Bao C, Zhu M, Nykonchuk I, Wakabayashi H, Mathews DH, Ermolenko DN. 2022. Specific length and structure rather than high thermodynamic stability enable regulatory mRNA stem-loops to pause translation. *Nat Commun* **13:** 988. doi:10.1038/s41467-022-28600-5

Bosco DA. 2018. Translation dysregulation in neurodegenerative disorders. *Proc Natl Acad Sci* **115:** 12842–12844. doi:10.1073/pnas.1818493115

Burke PC, Park H, Subramaniam AR. 2022. A nascent peptide code for translational control of mRNA stability in human cells. *Nat Commun* **13:** 6829. doi:10.1038/s41467-022-34664-0

Buskirk AR, Green R. 2017. Ribosome pausing, arrest and rescue in bacteria and eukaryotes. *Philos Trans R Soc Lond B Biol Sci* **372:** 20160183. doi:10.1098/rstb.2016.0183

Carroll JS, Munchel SE, Weis K. 2011. The DExD/H box ATPase Dhh1 functions in translational repression, mRNA decay, and processing body dynamics. *J Cell Biol* **194:** 527–537. doi:10.1083/jcb.201007151

Chan LY, Mugler CF, Heinrich S, Vallotton P, Weis K. 2018. Non-invasive measurement of mRNA decay reveals translation initiation as the major determinant of mRNA stability. *Elife* **7:** e32536. doi:10.7554/eLife.32536

Chu D, Barnes DJ, von der Haar T. 2011. The role of tRNA and ribosome competition in coupling the expression of different mRNAs in *Saccharomyces cerevi*siae. *Nucleic Acids Res* **39:** 6705–6714. doi:10.1093/nar/gkr300

Chu D, Kazana E, Bellanger N, Singh T, Tuite MF, von der Haar T. 2014. Translation elongation can control translation initiation on eukaryotic mRNAs. *EMBO J* **33:** 21–34. doi:10.1002/embj.201385651

Coller JM, Tucker M, Sheth U, Valencia-Sanchez MA, Parker R. 2001. The DEAD box helicase, Dhh1p, functions in mRNA decapping and interacts with both the decapping and deadenylase complexes. *RNA* **7:** 1717–1727. doi:10.1017/S135583820101994X

del Alamo M, Hogan DJ, Pechmann S, Albanese V, Brown PO, Frydman J. 2011. Defining the specificity of cotranslationally acting chaperones by systematic analysis of mRNAs associated with ribosome-nascent chain complexes. *PLoS Biol* **9:** e1001100. doi:10.1371/journal.pbio.1001100

D'Orazio KN, Wu CCC, Sinha N, Loll-Krippleber R, Brown GW, Green R. 2019. The endonuclease Cue2 cleaves mRNAs at stalled ribosomes during No Go Decay. *Elife* **8:** e49117. doi:10.7554/eLife.49117

dos Reis M, Savva R, Wernisch L. 2004. Solving the riddle of codon usage preferences: a test for translational selection. *Nucleic Acids Res* **32:** 5036–5044. doi:10.1093/nar/gkh834

Edwards AM, Kane CM, Young RA, Kornberg RD. 1991. Two dissociable subunits of yeast RNA polymerase II stimulate the initiation of transcription at a promoter *in vitro*. *J Biol Chem* **266:** 71–75. doi:10.1016/S0021-9258(18)52403-0

Ferrin MA, Subramaniam AR. 2017. Kinetic modeling predicts a stimulatory role for ribosome collisions at elongation stall sites in bacteria. *Elife* **6:** e23629. doi:10.7554/eLife.23629

Fischer N, Weis K. 2002. The DEAD box protein Dhh1 stimulates the decapping enzyme Dcp1. *EMBO J* **21:** 2788–2797. doi:10.1093/emboj/21.11.2788

Gamble CE, Brule CE, Dean KM, Fields S, Grayhack EJ. 2016. Adjacent codons act in concert to modulate translation efficiency in yeast. *Cell* **166:** 679–690. doi:10.1016/j.cell.2016.05.070

Gardin J, Yeasmin R, Yurovsky A, Cai Y, Skiena S, Futcher B. 2014. Measurement of average decoding rates of the 61 sense codons *in vivo*. *Elife* **3:** e03735. doi:10.7554/eLife.03735

Goldman DH, Livingston NM, Movsik J, Wu B, Goldman DH, Livingston NM, Movsik J, Wu B, Green R. 2021. Live-cell imaging reveals kinetic determinants of quality control triggered by ribosome stalling. *Mol Cell* **81:** 1830–1840.e8. doi:10.1016/j.molcel.2021.01.029

Han P, Shichino Y, Schneider-Poetsch T, Mito M, Hashimoto S, Udagawa T, Kohno K, Yoshida M, Mishima Y, Inada T, et al. 2020. Genome-wide survey of ribosome collision. *Cell Rep* **31:** 107610. doi:10.1016/j.celrep.2020.107610

Hanson G, Coller J. 2018. Codon optimality, bias and usage in translation and mRNA decay. *Nat Rev Mol Cell Biol* **19:** 20–30. doi:10.1038/nrm.2017.91

Harigaya Y, Parker R. 2016. Codon optimality and mRNA decay. *Cell Res* **26:** 1269–1270. doi:10.1038/cr.2016.127

Hartl FU, Bracher A, Hayer-Hartl M. 2011. Molecular chaperones in protein folding and proteostasis. *Nature* **475:** 324–332. doi:10.1038/nature10317

Hickey KL, Dickson K, Cogan JZ, Replogle JM, Schoof M, D'Orazio KN, Sinha NK, Hussmann JA, Jost M, Frost A, et al. 2020. GIGYF2 and 4EHP inhibit translation initiation of defective messenger RNAs to assist ribosome-associated quality control. *Mol Cell* **79:** 950–962.e6. doi:10.1016/j.molcel.2020.07.007

Hussmann JA, Patchett S, Johnson A, Sawyer S, Press WH. 2015. Understanding biases in ribosome profiling experiments reveals signatures of translation dynamics in yeast. *PLoS Genet* **11:** e1005732. doi:10.1371/journal.pgen.1005732

Ikeuchi K, Tesina P, Matsuo Y, Sugiyama T, Cheng J, Saeki Y, Tanaka K, Becker T, Beckmann R, Inada T. 2019. Collided ribosomes form a unique structural interface to induce Hel2-driven quality control pathways. *EMBO J* **38:** e100276. doi:10.15252/embj.2018100276

Ingolia NT. 2014. Ribosome profiling: new views of translation, from single codons to genome scale. *Nat Rev Genet* **15:** 205–213. doi:10.1038/nrg3645

Ingolia NT, Ghaemmaghami S, Newman JRS, Weissman JS. 2009. Genome-wide analysis *in vivo* of translation with nucleotide resolution using ribosome profiling. *Science* **324:** 218–223. doi:10.1126/science.1168978

Joazeiro CAP. 2017. Ribosomal stalling during translation: providing substrates for ribosome-associated protein quality control. *Annu Rev Cell Dev Biol* **33:** 343–368. doi:10.1146/annurev-cellbio-111315-125249

Jungfleisch J, Nedialkova DD, Dotu I, Sloan KE, Martinez-Bosch N, Brüning L, Raineri E, Navarro P, Bohnsack MT, Leidel SA, et al. 2017. A novel translational control mechanism involving RNA structures within coding sequences. *Genome Res* **27:** 95–106. doi:10.1101/gr.209015.116

Karpinets T V, Greenwood DJ, Sams CE, Ammons JT. 2006. RNA:protein ratio of the unicellular organism as a characteristic of phosphorous and nitrogen stoichiometry and of the cellular requirement of ribosomes for protein synthesis. *BMC Biol* **4:** 30. doi:10.1186/1741-7007-4-30

Koutmou KS, Radhakrishnan A, Green R. 2015. Synthesis at the speed of codons. *Trends Biochem Sci* **40:** 717–718. doi:10.1016/j.tibs.2015.10.005

Letzring DP, Dean KM, Grayhack EJ. 2010. Control of translation efficiency in yeast by codon–anticodon interactions. *RNA* **16:** 2516–2528. doi:10.1261/rna.2411710

Liu X, Yao Z, Jin M, Namkoong S, Yin Z, Lee JH, Klionsky DJ. 2019. Dhh1 promotes autophagy-related protein translation during nitrogen starvation. *PLoS Biol* **17:** e3000219. doi:10.1371/journal.pbio.3000219

Mason PB, Struhl K. 2005. Distinction and relationship between elongation rate and processivity of RNA polymerase II *in vivo*. *Mol Cell* **17:** 831–840. doi:10.1016/j.molcel.2005.02.017

Masser AE, Kandasamy J, Kaimal M, Andreasson C. 2016. Luciferase NanoLuc as a reporter for gene expression and protein levels in *Saccharomyces cerevisiae*. *Yeast* **26:** 191–200. doi:10.1002/yea.3155

Maton N, Ciufo LF, Brown JD. 2000. Elongation arrest is a physiologically important function of signal recognition particle. *EMBO J* **19:** 4164–4174. doi:10.1093/emboj/19.15.4164

Matsuo Y, Ikeuchi K, Saeki Y, Iwasaki S, Schmidt C, Udagawa T, Sato F, Tsuchiya H, Becker T, Tanaka K, et al. 2017. Ubiquitination of stalled ribosome triggers ribosome-associated quality control. *Nat Commun* **8:** 159. doi:10.1038/s41467-017-00188-1

Meydan S, Guydosh NR. 2020. Disome and trisome profiling reveal genome-wide targets of ribosome quality control. *Mol Cell* **79:** 588–602.e6. doi:10.1016/j.molcel.2020.06.010

Meydan S, Guydosh NR. 2021. A cellular handbook for collided ribosomes: surveillance pathways and collision types. *Curr Genet* **67:** 19–26. doi:10.1007/s00294-020-01111-w

Navickas A, Chamois S, Saint-Fort R, Henri J, Torchet C, Benard L. 2020. No-Go Decay mRNA cleavage in the ribosome exit tunnel produces 5′-OH ends phosphorylated by Trl1. *Nat Commun* **11:** 122. doi:10.1038/s41467-019-13991-9

Ogg SC, Walter P. 1995. SRP samples nascent chains for the presence of signal sequences by interacting with ribosomes at a discrete step during translation elongation. *Cell* **81:** 1075–1084. doi:10.1016/S0092-8674(05)80012-1

Park H, Subramaniam AR. 2019. Inverted translational control of eukaryotic gene expression by ribosome collisions. *PLoS Biol* **17:** e3000396. doi:10.1371/journal.pbio.3000396

Pechmann S, Frydman J. 2013. Evolutionary conservation of codon optimality reveals hidden signatures of cotranslational folding. *Nat Struct Mol Biol* **20:** 237–243. doi:10.1038/nsmb.2466

Pechmann S, Willmund F, Frydman J. 2013. The ribosome as a hub for protein quality control. *Mol Cell* **49:** 411–421. doi:10.1016/j.molcel.2013.01.020

Presnyak V, Alhusaini N, Graveley BR, Coller J, Presnyak V, Alhusaini N, Chen Y, Martin S, Morris N, Kline N, et al. 2015. Codon optimality is a major determinant of mRNA article. *Cell* **160:** 1111–1124. doi:10.1016/j.cell.2015.02.029

Radhakrishnan A, Chen Y-H, Martin S, Alhusaini N, Green R, Coller J. 2016. The DEAD-box protein Dhh1p couples mRNA decay and translation by monitoring codon optimality. *Cell* **167:** 122–132.e9. doi:10.1016/j.cell.2016.08.053

Riba A, Di Nanni N, Mittal N, Arhné E, Schmidt A, Zavolan M. 2019. Protein synthesis rates and ribosome occupancies reveal determinants of translation elongation rates. *Proc Natl Acad Sci* **116:** 15023–15032. doi:10.1073/pnas.1817299116

Saikia M, Wang X, Mao Y, Wan J, Pan T, Qian S-B. 2016. Codon optimality controls differential mRNA translation during amino acid starvation. *RNA* **22:** 1719–1727. doi:10.1261/rna.058180.116

Schleif R, Hess W, Finkelstein S, Ellis D. 1973. Induction kinetics of the L-arabinose operon of *Escherichia coli*. *J Bacteriol* **115:** 9–14. doi:10.1128/jb.115.1.9-14.1973

Shah P, Ding Y, Niemczyk M, Kudla G, Plotkin JB. 2013. Rate-limiting steps in yeast protein translation. *Cell* **153:** 1589–1601. doi:10.1016/j.cell.2013.05.049

Simms CL, Yan LL, Zaher HS. 2017. Ribosome collision is critical for quality control during no-go decay. *Mol Cell* **68:** 361–373.e5. doi:10.1016/j.molcel.2017.08.019

Sonenberg N, Hinnebusch AG. 2009. Regulation of translation initiation in eukaryotes: mechanisms and biological targets. *Cell* **136:** 731–745. doi:10.1016/j.cell.2009.01.042

Spencer PS, Siller E, Anderson JF, Barral JM. 2012. Silent substitutions predictably alter translation elongation rates and protein folding efficiencies. *J Mol Biol* **422:** 328–335. doi:10.1016/j.jmb.2012.06.010

Stein KC, Frydman J. 2019. The stop-and-go traffic regulating protein biogenesis: how translation kinetics controls proteostasis. *J Biol Chem* **294:** 2076–2084. doi:10.1074/jbc.REV118.002814

Sweet T, Kovalak C, Coller J. 2012. The DEAD-box protein Dhh1 promotes decapping by slowing ribosome movement. *PLoS Biol* **10:** e1001342. doi:10.1371/journal.pbio.1001342

Tesina P, Lessen LN, Buschauer R, Cheng J, Wu CC, Berninghausen O, Buskirk AR, Becker T, Beckmann R, Green R. 2020. Molecular mechanism of translational stalling by inhibitory codon combinations and poly(A) tracts. *EMBO J* **39:** e103365. doi:10.15252/embj.2019103365

Tseng-Rogenski SS-I, Chong J-L, Thomas CB, Enomoto S, Berman J, Chang T-H. 2003. Functional conservation of Dhh1p, a cytoplasmic DExD/H-box protein present in large complexes. *Nucleic Acids Res* **31:** 4995–5002. doi:10.1093/nar/gkg712

Tsuboi T, Kuroha K, Kudo K, Makino S, Inoue E, Kashima I, Inada T. 2012. Dom34: Hbs1 plays a general role in quality-control systems by dissociation of a stalled ribosome at the 3′ end of aberrant mRNA. *Mol Cell* **46:** 518–529. doi:10.1016/j.molcel.2012.03.013

Tsuboi T, Viana MP, Xu F, Yu J, Chanchani R, Arceo XG, Tutucci E, Choi J, Chen YS, Singer RH, et al. 2020. Mitochondrial volume fraction and translation speed impact mRNA localization and production of nuclear-encoded mitochondrial proteins. *Elife* **9:** e57814. doi:10.7554/eLife.57814

Veltri AJ, D'orazio KN, Lessen LN, Loll-Krippleber R, Brown GW, Green R. 2022. Distinct elongation stalls during translation are linked with distinct pathways for mRNA degradation. *Elife* **11:** e76038. doi:10.7554/eLife.76038

Wang ET, Taliaferro JM, Lee JA, Sudhakaran IP, Rossoll W, Gross C, Moss KR, Bassell GJ. 2016. Dysregulation of mRNA localization and translation in genetic disease. *J Neurosci* **36:** 11418–11426. doi:10.1523/JNEUROSCI.2352-16.2016

Weinberg DE, Shah P, Eichhorn SW, Hussmann JA, Plotkin JB, Bartel DP. 2016. Improved ribosome-footprint and mRNA measurements provide insights into dynamics and regulation of yeast translation. *Cell Rep* **14:** 1787–1799. doi:10.1016/j.celrep.2016.01.043

Yip MCJ, Shao S. 2021. Detecting and rescuing stalled ribosomes. *Trends Biochem Sci* **46:** 731–743. doi:10.1016/j.tibs.2021.03.008

Yu CH, Dang Y, Zhou Z, Wu C, Zhao F, Sachs MS, Liu Y. 2015. Codon usage influences the local rate of translation elongation to regulate co-translational protein folding. *Mol Cell* **59:** 744–754. doi:10.1016/j.molcel.2015.07.018

Zhao T, Chen YM, Li Y, Wang J, Chen S, Gao N, Qian W. 2021. Disome-seq reveals widespread ribosome collisions that recruit co-translational chaperones. *Genome Biol* **22:** 16. doi:10.1186/s13059-020-02256-0